Dilatancy, buckling, and undulations on a vertically vibrating granular layer

Osamu Sano
Department of Applied Physics, Tokyo University of Agriculture and Technology, Koganei, Tokyo 184-8588, Japan
(Received 21 June 2005; published 11 November 2005)

We report experiments on a vertically vibrated quasi-two-dimensional granular layer of lead spheres showing subharmonic undulations and ripples, which are associated with horizontal dilatation at the impingement of the bottom wall. By systematically changing frequency and amplitude of external forcing, as well as the container sizes and layer height, we observed various eigenmodes of undulations, whose selection is determined by the amount of configuration changes in densely packed particles along the bottom wall. Resulting enhancement of horizontal stress induces the buckling and bending of the granular layer of successively higher modes.

DOI: 10.1103/PhysRevE.72.051302 PACS number(s): 45.70.Qj, 47.54.+r, 83.10.Pp

I. INTRODUCTION

Pattern formation on the vibrating granular layer, such as heap formation and convection, size segregations, bubbling, and subharmonic standing waves, either in three-dimensional (3D) or in two-dimensional (2D) systems, has attracted much attention since the pioneering work of Faraday [1–4]. The standing waves include archlike deformation [5–8] and surface waves [9–18], which are designated as "undulations" and "ripples," respectively, in our terminology [19–21], the latter are local and independent of the container size, whereas the former have large length scale and can depend on the system size.

The "ripple" patterns, like square, stripe, and hexagonal cells, etc. are often and successfully classified on the pattern diagram in the $\Gamma - f^*$ plane ($\Gamma \equiv 4\pi^2 f^2 a/g$ and $f^* \equiv f\sqrt{h/g}$, where f and a are, respectively, the frequency and amplitude of external forcing, and h is the layer height defined by the volume of granular material divided by the horizontal cross section). The dispersion relation is also scaled by h. A question arises whether the same behavior is realized for the layers with a given height h and different layer numbers $N \equiv h/d$ (d is the diameter of the particle). Apparently this is not the case when the mean layer number N approaches to or becomes less than unity. In the latter, collision among the particles becomes very scarce, so that no collective motion is expected. In fact, we have revealed that the configuration changes of densely packed particles at the time of impingement on the bottom wall are essential to the generation of wave patterns, and that the number of layers that any kind of pattern is recognized is found to be at least about three, i.e., roughly speaking, the lowest layer that is pushed up by the bottom wall, the second layer that undergoes intrusion of the lowest one, and the third one that suppresses the complete free flight of the layers below. This means that the layer number N and hence the microscopic scale d is important when we consider the transition of the system from "solid" to "fluid" phases, but that the macroscopic scale h becomes dominant, once the wave motion fully develops [19,21].

Another type of collective motion "undulations" can also be observed in the same $\Gamma - f^*$ regions as those of ripples, which shows that the classification by means of Γ and f^* is not sufficient in this case. These complexities may be partly attributed to the presence of other unspecified experimental conditions, and partly due to the necessity of including particle size d depending on whether the system is in solidlike or fluidlike states. Thus when the pattern diagram in the $\Gamma - f^*$ plane is plotted, differences in relative oscillation amplitude a/d and the relative phase between the layer and the container, aspect ratios of the container L/d and W/d (L and W are the sizes of the container in horizontal cross section), number of layers N, in addition to the difference of granular materials, are discarded, which makes it difficult to compare available experimental data and/or numerical simulations of different workers. It is, therefore, important to understand the effect of each factor on the pattern formation of granular material, and to reduce the number of relevant parameters, or to derive a proper scaling relation for a given collective motion. To this end we have examined the characteristics of quasi-two-dimensional (Q2D) undulations of a thin granular layer induced by vertical vibration [19–21]. In particular, we checked the effects of the layer height h and the separation distance W of the vertical walls whose magnitude changed down to as small as one particle diameter size, whereas the other horizontal extension L was kept sufficiently large compared to the wavelength of the pattern [21]. We elucidated the fundamental characteristics in 2D or Q2D wave motions of the layer, i.e., "undulations" and "ripples," and found that "regular pattern of defects" [5], "several regions that move out of phase with each other and are separated by nodes" [6,7], "transverse bending" [8], "array of peaked structure" [13,15], "phase bubbles," "$f/2$ flat pattern with a kink," and "$f/4$ pattern with kinks" [18] fall into the same category, which we shall term "undulations" [20,21]. On the other hand, the pattern forming instabilities observed in a vertically vibrating thin granular layer with 3D geometry [1,9–12] or those with 2D geometry [13–18] are associated with "ripples," the latter being interpreted as vertical cross section of the former.

Our observation using a high-speed video camera shows that the particle trajectories of the ripples relative to the container are more or less a figure-eight shape, suggesting that the whole system is in a fluid state, whereas those of undulations are nearly vertical, suggesting that the system behaves like bending of a single elastic layer. In the latter, local

alignment of the particles on the container wall necessarily induces the horizontal dilatation, which is decisive to the onset of undulations [21]. There still remains a question how the higher undulation modes are produced. In this paper we show our experimental results on the various modes of undulations, behavior of particles at the impingement of the layer on the bottom wall, and propose a continuum model that takes account of the amount of dilatation due to configuration change in a particle-size level.

II. EXPERIMENT

We performed experiments on the pattern formation of a vertically oscillated layer of granular material consisting of spherical lead particles of mean diameter $d=1.0$ mm under atmospheric pressure. The particles were filled to the depth h in a container of rectangular cross section L and W, which was mounted on an electromagnetic shaker. We used three types of container (C1) $L=100$ mm, $W=10$ mm, (C2) $L=140$ mm, $W=3$ mm, and (C3) $L=30$ mm, $W=5$ mm, which we had tested in our previous work [21] that Q2D dynamics on the pattern formation was relevant. The container was oscillated with a single frequency, and the patterns were observed from the side by a high-speed video camera. A more detailed description of the experimental apparatus is found in Refs. [19–21].

We show some examples of undulation modes in Figs. 1(a)–1(j) and that of ripples in Fig. 1(k). Each undulation pattern repeated with a frequency $f/2$, or the pattern which shifted half wavelength appeared after a time $T\equiv 1/f$, whereas the ripples in this example repeated with $f/4$. The container types used were (C1) for Figs. 1(a)–1(g) and 1(k), and (C2) for Figs. 1(h)–1(j). Various undulation modes, in which a discrete number of arches are formed between the sidewalls of the container, were recognized and were denoted by A_M and S_M [20] as the pattern is antisymmetric and symmetric, respectively, with respect to the center of the layer and M is the number of undulations. In our terminology, the pattern described in Fig. 3(a) of Ref. [5] belongs to A_2.

Figure 2 is an example of the time trajectory of a marker particle in the lowest layer in undulation mode. In steady undulations, the layer of particles touches the bottom wall when it is nearly at rest at its highest position ($z\approx a$), and is carried downward with the movement of the bottom wall. The layer of particles is then pushed up by the bottom wall, where upward momentum is given during the period nearly equal to $T/2$. The temporal trajectory resembles that of the $f/4$-square/stripe regime described by Bizon *et al.* [17] or that of $f/4$-hexagonal pattern regime or phase bubble described by Moon *et al.* [18], as far as the timing of collision (and not the number of oscillations) is concerned.

We show the pattern diagram in the $\Gamma - f^*$ plane in Fig. 3. The region of our $f/4$-ripples agrees with available data [17,18], although the latter were obtained in planar pattern formation. On the other hand, the undulation modes are distributed in larger Γ and f^* values, but are not well categorized in this diagram.

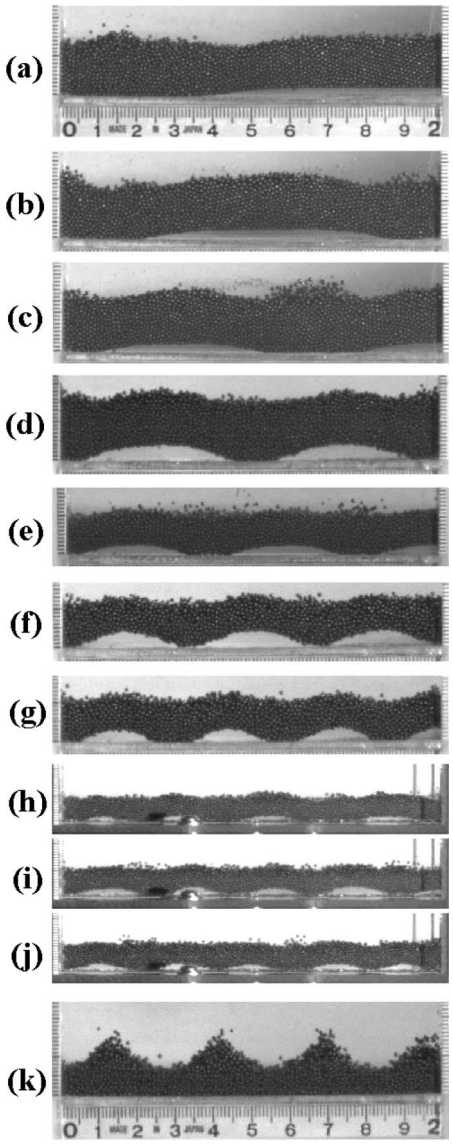

FIG. 1. Patterns observed in vertically vibrating lead spheres of diameter $d=1.0$ mm: undulation modes, (a) $A_1(f=45$ Hz$,a=0.61$ mm$,h=12.0$ mm), (b) $S_1(f=45$ Hz$,a=0.82$ mm$,h=12.0$ mm), (c) $A_2(f=50$ Hz$,a=0.82$ mm$,h=12.0$ mm), (d) $S_2(f=40$ Hz$,a=1.25$ mm$,h=13.0$ mm), (e) $A_3(f=48$ Hz$,a=0.83$ mm$,h=8.7$ mm), (f) $S_3(f=40$ Hz$,a=1.26$ mm$,h=7.8$ mm), (g) $A_4(f=45$ Hz$,a=1.11$ mm$,h=7.8$ mm), (h) $S_4(f=50$ Hz$,a=0.76$ mm$,h=6.9$ mm), (i) $A_5(f=45$ Hz$,a=0.90$ mm$,h=6.9$ mm), (j) $S_5(f=50$ Hz$,a=0.90$ mm$,h=6.9$ mm), and (k) ripples ($f=32.5$ Hz, $a=1.49$ mm, $h=7.8$ mm). The sizes of the container are $L=100$ mm for (a)–(g) and (k), whereas $L=140$ mm for (h)–(j).

III. CONFIGURATION CHANGE IN UNDULATIONS

A. Configuration changes at the impingement on the bottom wall

We show the close up view of the undulation mode in Fig. 4. Particle positions, relative to the frame of reference moving with the container, are described by the circles. Frame speed of the high-speed video camera is 1/1000 s, and five snapshots are superposed in each picture of Figs. 4(a)–4(c).

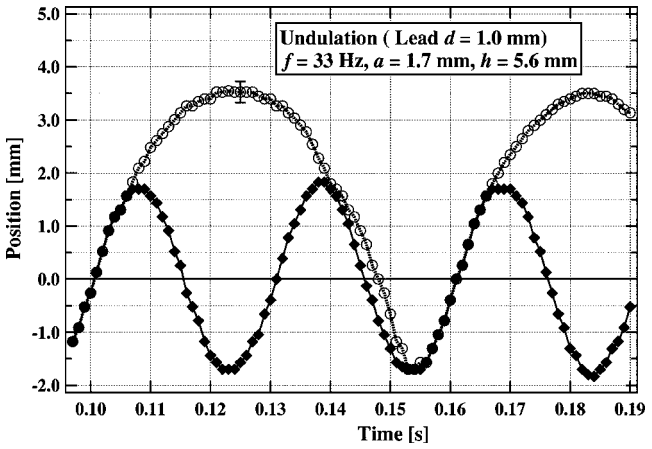

FIG. 2. Time trajectory of a marker particle in the lowest layer in undulation mode ($f=33$ Hz, $a=1.7$ mm, $h=5.6$ mm; $f^*=0.79$, $\Gamma=7.5$). Observation was made for an oscillated monolayer of lead spheres. Open circles and dotted line show the orbit of the marker particle, whereas closed diamonds and solid lines show the movement of the bottom wall.

Thus the discernible circles show particles which remain almost at rest over 4 ms. When some particles in the lowest layer collide with the bottom wall [Fig. 4(a)], they align along the wall and solidify with closest packing [Fig. 4(b)]. The resulting dilatation in horizontal directions, e.g., the configuration change from Fig. 4(d) and 4(e) yields the horizontal dilatation by $2/\sqrt{3}\approx 1.15$ times, inevitably causes undulations of the layer. (Note that this will not be the case in "ripple" formation, where all the particles above the second ones can also ascend.) When the particles first collided with the bottom wall are pushed up to have sufficient curvature, the compaction in this region is relaxed, so that the density wave propagates in both directions along the layer [Fig. 4(c)]. Similar behavior was reported experimentally by Douady *et al.* [5] who described it as "kink-type defect" and numerically by Moon *et al.* [18] in their "$f/2$ flat pattern with a kink," where the density waves or a momentum transfer propagation along the layer was shown. As has been shown previously [21] each particle moves nearly vertically in the layer, except a slight inclination, at the time of impingement on the bottom wall.

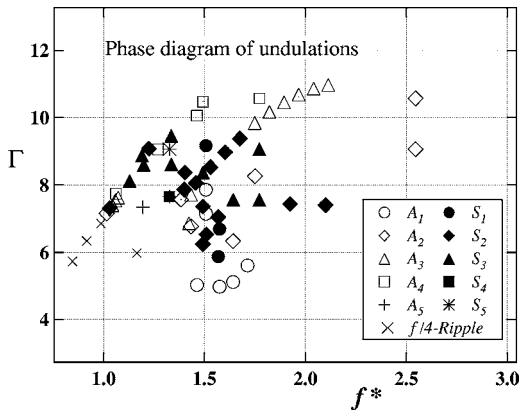

FIG. 3. Phase diagram for undulations and $f/4$-ripples obtained in our experiments.

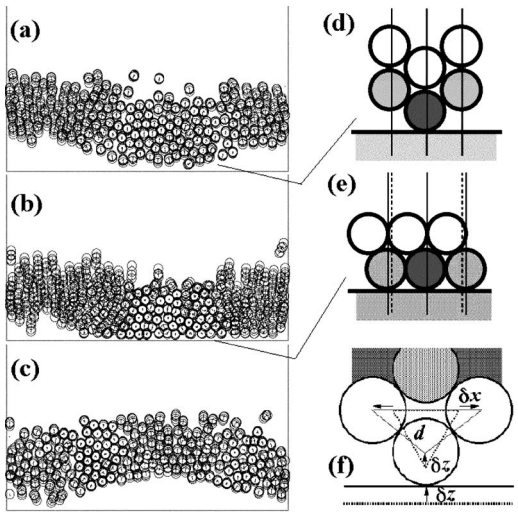

FIG. 4. Particle behavior in undulation mode. Lead spheres of diameter $d=1.0$ mm and layer height $h=5.6$ mm are exposed to sinusoidal oscillation of frequency $f=40$ Hz and amplitude $a=1.2$ mm ($f^*\equiv f\sqrt{h/g}=0.96$, $\Gamma=7.7$). Superposition of particle contours of five snapshots; (a) $t=0-4$ ms, (b) $t=10-14$ ms, and (c) $t=25-29$ ms. Time interval between (a) and (c) is one period of external oscillation ($=1/f$). Schematic pictures (d) and (e) show the configuration changes when the layer collides with the bottom wall, and (f) horizontal dilatation due to intrusion of the bottom layer into the second one.

B. Dilatancy and buckling of the granular layer at the impingement on the bottom wall

We shall consider the horizontal dilatation of the layer induced by the impingement on the bottom wall. Let us assume, for simplicity, that the particles in the lowest layer intrude vertically into adjacent particles by the amount δz, but that the upward motion of the latter is suppressed by the rest of the particles above the second layer as shown in Fig. 4(f). Resulting horizontal increment δx is given by

$$\delta x = \sqrt{d^2 - \left(\frac{\sqrt{3}}{2}d - \delta z\right)^2} - \frac{d}{2}. \tag{1}$$

The number of particles n initially aligned on the bottom layer is given by $n=L/d$, so that the total increment of the layer ΔL is $\Delta L=2(n-1)\delta x$, which is approximately given by

$$\Delta L \approx 2\sqrt{3}L\frac{\delta z}{d}, \tag{2}$$

for $n\gg 1$ and $\delta z \ll d$. The stress f_H acting along the layer is given by

$$f_H = \tilde{E}\frac{\Delta L}{L} = 2\sqrt{3}\tilde{E}\frac{\delta z}{d}, \tag{3}$$

where $\tilde{E}$ is an effective Young's modulus of the layer determined by this relation. (The meaning of Young's modulus needs a caution, which we shall discuss later.) If the stress exceeds a certain threshold value, buckling will occur, and an archlike structure will be formed between the side walls of fixed distance L [see Figs. 5(a)–5(c)].

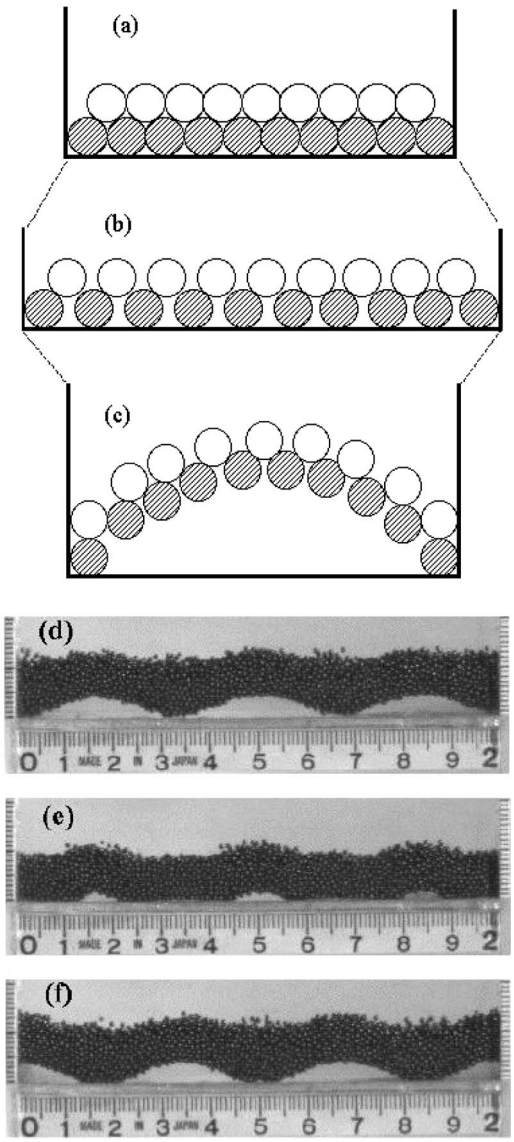

FIG. 5. (a)–(c) Archlike structure due to horizontal dilatation, and various phases in multiarches (S_3 mode): (d) $t^*=0$, (e) $t^*=0.48$, and (f) $t^*=1.12$, where $t^*=ft$.

Let us consider the deformation of an elastic layer of initial length L, width W, and height h, due to the force F applied normally to both ends of the layer. The basic equation of the deformation is (see, for example, Ref. [24])

$$\frac{d^2\theta}{ds^2} = -\alpha^2 \sin\theta, \tag{4}$$

where $\alpha=\sqrt{F/\tilde{E}I}$, and $I(\equiv Wh^3/12)$ is the moment of inertia of the cross-sectional area. Here s is the length of the layer measured from one of its end, at which the origin of the x and z axes (taken in the horizontal and vertical directions, respectively) is chosen. We also introduce θ, which describes the angle tangent to the arc measured from the x axis. By integrating Eq. (4) we obtain

$$\alpha s = \pm \int_0^{\varphi} \frac{d\varphi}{\sqrt{1-k^2\sin^2\varphi}} \equiv F(\varphi,k), \tag{5}$$

where we have assumed $d\theta/ds=0$ and $\theta=\theta_0$ at a certain position $s=s_0$, and $\theta=0$, $\varphi=0$ at $s=0$. Here we have defined

$$\sin\left(\frac{\theta}{2}\right) = k\sin\varphi, \quad k=\sin\left(\frac{\theta_0}{2}\right), \tag{6}$$

and $F(\varphi,k)$ is the elliptic integral of the first kind. Integration of the relation

$$\frac{dz}{ds} = \sin\theta = 2\sin\left(\frac{\theta}{2}\right)\cos\left(\frac{\theta}{2}\right) = 2k\,\mathrm{sn}(\alpha s)\mathrm{dn}(\alpha s)$$

$$= -\frac{2k}{\alpha}\frac{d}{ds}\mathrm{cn}(\alpha s)$$

gives us

$$z = \frac{2k}{\alpha}[1-\mathrm{cn}(\alpha s)], \tag{7}$$

where $\mathrm{sn}(\alpha s)$, $\mathrm{cn}(\alpha s)$, and $\mathrm{dn}(\alpha s)$ are the Jacobi's elliptic functions defined by

$$\sin\varphi = \sin[\mathrm{am}(\alpha s)] = \mathrm{sn}(\alpha s),$$

$$\cos\varphi = \mathrm{cn}(\alpha s), \quad \mathrm{dn}(\alpha s) = \sqrt{1-k^2\,\mathrm{sn}^2(\alpha s)}$$

and $\varphi=\mathrm{am}(\alpha s)$, called the "amplitude," is the inverse function of $F(\varphi,k)$. Similarly by integrating the relation

$$\frac{dx}{ds} = \cos\theta = 1-2k^2\,\mathrm{sn}^2(\alpha s) = 2\,\mathrm{dn}^2(\alpha s) - 1,$$

we obtain

$$x = \frac{2}{\alpha}\left[E(\mathrm{am}(\alpha s),k) - \frac{1}{2}\alpha s\right]$$

$$= \frac{2}{\alpha}\left[Z(\mathrm{am}(\alpha s),k) + \left(\frac{E}{K}-\frac{1}{2}\right)\alpha s\right], \tag{8}$$

where $E(\varphi,k)$ and $Z(\varphi,k)$ are the elliptic integral of the second kind and the Jacobi's zeta elliptic function, respectively, whereas $K(k)$ and $E(k)$ are the complete elliptic integrals of the first and second kind, respectively. Note that $E(\varphi,k)$ is not periodic, but the function $Z(\varphi,k)$ is singly periodic of period $2K(k)$ [25]. Our experiment shows that the other end of the layer also meets perpendicularly to the side wall at $x=L$. This condition requires $\alpha s=2M^*K(k)$, where odd and even integers of M^* correspond to antisymmetric modes and symmetric modes, respectively. In both cases $Z(\varphi,k)$ vanishes at the end point of the layer (i.e., at the sidewall), so that the above conditions give

$$\alpha L = 2M^*[2E(k)-K(k)]. \tag{9}$$

We show examples of the layer shape in Fig. 6, which qualitatively agree with those of the bottom contour of the layer in Fig. 1.

Our scenario is as follows: given the rate of intrusion of the layer of particles at the impingement $\delta z/d$, the dilatation

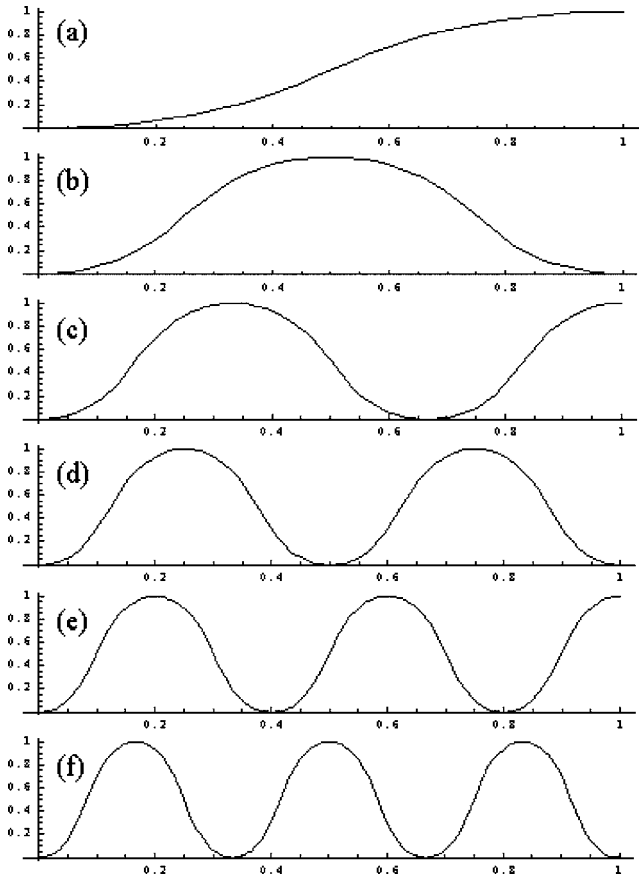

FIG. 6. Calculated undulation modes with $k=0.5$. The abscissa is x/L and the ordinate is z in arbitrary unit. (a) A_1, (b) S_1, (c) A_2, (d) S_2, (e) A_3, and (f) S_3.

in the horizontal direction $\Delta L/L$ is calculated by Eq. (2) which determines the force F applied perpendicularly to the layer, and hence the parameter α. Then the mode M^* is determined by Eq. (9), and so is the layer shape by Eqs. (7) and (8).

Note that the lowest mode $M^*=1$ gives the critical force F_c given by

$$F_c = \tilde{E}I\left(\frac{\pi}{L}\right)^2. \tag{10}$$

For smaller k, we have

$$k \approx \sqrt{\frac{4}{3}\left(1-\frac{\alpha L}{\pi}\right)} \propto \sqrt{\frac{F-F_c}{F_c}}, \tag{11}$$

and

$$M^* = \frac{\alpha L}{2(2E-K)} = \frac{\alpha L}{\pi}\left(1+\frac{3}{4}k^2+\cdots\right) \approx \frac{2L}{\pi h}\sqrt{6\sqrt{3}\frac{\delta z}{d}}. \tag{12}$$

C. Estimation of $\delta z/d$

The value of $\delta z/d$ may depend on the impact velocity, as well as the properties of the particle, which we shall estimate in the following. Generally speaking, the pattern formation of granular beds vibrating vertically like $z=a\sin(2\pi ft)$, can occur if a finite period of lift-off phase is present, which is larger than $\arcsin(1/\Gamma)$ for a single particle. In the particulate dissipative system, however, a still larger threshold acceleration must be necessary above which the uppermost particles in the layer acquire freeflight motion. The whole layer will then be in fluidlike state and can develop into " ripples." On the other hand, if the layer has a lift-off phase but the upward momentum is dissipated before it is transmitted to the uppermost particles, the whole layer moves up-and-down, possibly showing local relative motions, but will remain an undulating layer. Our observation shows that soft-landing and soft-release of particles, where the colliding phase $2\pi ft$ is $2\pi(7/4+\varepsilon_u)$ with $\varepsilon_u \approx 0.03$ as is typically shown in Fig. 2 (and also in Ref. [20] for other granular material), lead to "undulations." On the contrary, hard hitting of the layer on the bottom wall, which occurs around $2\pi(2-\varepsilon_r)$ with $\varepsilon_r \approx 0.06$, results in "ripples," as is shown in Ref. [19]. Consequently the lift-off velocity $V=2\pi fa\cos(2\pi ft)$ of the lowest layer of particles becomes about $0.2\times 2\pi fa$ for undulations, and $0.9\times 2\pi fa$ for ripples. Either of the two above-mentioned collision processes remains stable, through self-adjustment of the macroscopic wave motion to the externally applied oscillation of the vessel, whose detailed mechanism is not yet fully understood.

In the undulation mode, each particle in the lowest layer will thrust into the granular particles above it against the frictional force proportional to μmg, where μ is an effective friction coefficient and m is the mass of the particle. Here we have assumed that only a few layers of particles adjacent to the bottom layer are relevant to the contact forces due to local equilibrium of forces. The intrusion of the particle will be stopped when the kinetic energy of the particle is dissipated by the friction, so that

$$\frac{1}{2}mV^2 = C\mu mg\,\delta z, \tag{13}$$

where C is a constant as a first approximation. These assumptions lead us to

$$\frac{L}{\lambda} \propto M^* \propto \frac{L}{h}\frac{fa}{\sqrt{\mu gd}}. \tag{14}$$

We show our experimental results for undulation modes in Fig. 7. The ordinate is L/λ whereas the abscissa is $(L/h)[fa/\sqrt{gd}]$. Agreement is generally good. Larger deviation of L/λ for lower modes like A_1 and S_1 is mostly due to the finite size effect of the container. In fact it is difficult to rigorously determine which part of the layer touching the bottom wall belongs dynamically to one wavelength. On the other hand, scattering of the data in the abscissa seems to be ascribed to the variation of lift-off phase, as well as to the ambiguities of determining effective layer height h, which was measured at static state in this paper.

IV. DISCUSSION

Earlier observation of the similar pattern, which was termed "regular pattern of defects" [5], was interpreted as a

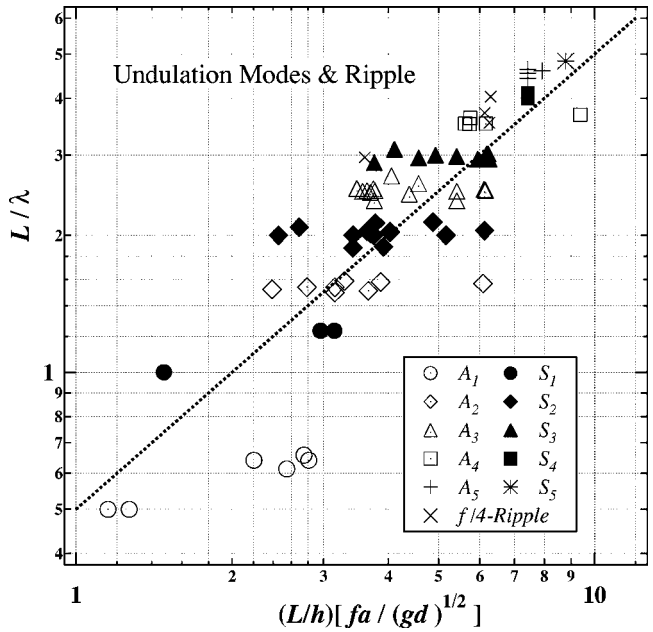

FIG. 7. Mode map. Symbols for A_1, S_1, A_2, S_2, A_3, … are shown in the inset.

result of the repulsive force between two defects or between a defect and the lateral boundary. In our experiment, we have elucidated that this "repulsive force" is given by the horizontal dilatation due to microscopic configuration change at the impingement on the bottom wall. We have also reproduced the tendency of h/λ on Γ [i.e., relation $H/l \approx 0.16(\Gamma - 4.2)$ of Ref. [5]], but our data are rather distributed around this curve, with the proportional coefficient being smaller (≈ 0.06) and the ordering of the undulation modes being mixed on this diagram. This is probably because Γ is necessary but not a sufficient control parameter to specify the system, apart from the difference of granular material.

All the results shown here are based on the data, which were obtained by abruptly applying an oscillation with prescribed frequency f and amplitude a to the granular layer initially at rest. By this procedure we determined the critical frequency f_c and critical amplitude a_c below which no undulation pattern was observed. Our undulation pattern has hysteresis, as is the case in most of the pattern formation in dissipative systems (e.g., [5,10,13]). In fact we sometimes observed undulations below f_c or a_c when we decreased f or a continuously after attaining some undulation mode. Conversely we did not necessarily observe undulations above f_c or a_c by continuously increasing f or a. These evidences suggest the difference of quasiequilibrium states of granular assemblies. When the layer moves up-and-down without considerably changing relative position of the constituents, it remains to be in a solid state, and does not show undulation modes. On the other hand the whole layer becomes a liquid state once the ripple mode sets in, and does not show undulations.

In this paper we have introduced an effective Young's modulus to explain buckling and bending of the granular layer. Our material, i.e. lead spheres, is noncohesive, so that the Young's modulus is not the same as that of ordinary solids. It is not surprising, however, that a particulate system with noncohesive or repulsive forces shows elastic behavior if the system is confined in finite boundaries [22]. In order to check our conjecture, we performed a simple experiment using the same apparatus, in which one of the sidewalls was replaced by sponge rubber of constant thickness. By measuring the deformation of the sponge rubber due to the stress exerted by a vertically oscillating granular layer, we can roughly estimate $\tilde{E} \approx 10^3$[Pa] for a layer with $h=10.3$ mm under external forcing $f=40$ Hz and $a=1.2$ mm, which is quite small in comparison to that of iron ($\tilde{E} \approx 2 \times 10^{11}$[Pa] and rubber ($\tilde{E} \approx 3 \times 10^6$[Pa]). In our previous paper [20], we have estimated the effective Young's modulus of the sesame layer as $\tilde{E} \approx 2 \times 10^4$[Pa] on the basis of the velocity of density waves in the granular layer, which is one order of magnitude larger than the present case. The difference will be attributed to a larger friction and nonspherical shape of the sesame to reduce relative translation and rotation, so that the cohesion and energy dissipation are enhanced. The effective Young's modulus of our system may depend on the external forcing f, a and the layer height h as well as the properties of the particle, such as density, friction coefficient, restitution coefficient, size and shape, etc. A closer look of our additional experiment reveals that it is only the particles in the lower part of the layer that exhibit the deformation of the sidewall, which is consistent with our findings [21] that this part plays a decisive role for the dilatation at the impingement, and hence contributes to undulations. In that case the effective Young's modulus will weakly depend on the layer height h as far as it exceeds a certain threshold value around $5d$ for lead spheres. The influence of the other factors is left for future investigations.

We observed patterns, in which $f/4$ ripples were accompanied by undulation slightly below A_1 or S_1 regions, which is similar to the 3D ones shown by Fig. 3 of Ref. [18]. In the latter "phase bubbles" is transient and shrinks with decay time depending on Γ and system size. On the other hand, our 2D pattern also changed the position of the kinks irregularly, but it developed over the layer with the increase of acceleration, to form stationary undulations. This apparent difference is resolved if we consider the different parameter values of Ref. [18], which are estimated to be $L/\lambda \approx 2$ and $(L/h)[fa/\sqrt{gd}] \approx 15$, the latter being much larger than the value we report here.

We have not mentioned ripple patterns because they have been fully discussed [1,9–21]. As has been shown in Fig. 1(k), ripples are also generated by the configuration change, in which the horizontal dilatation triggers the movement of the particle in the lower layer into the above ones. This can happen when the particles acquire large enough upward momentum depending on the external forcing such as f, a and the timing of collision with the bottom layer, against the dissipation depending on the friction and restitution coefficients of the material and the number of layers, etc. Once the ripples are generated, the whole system is in a fluid state, so that the wave motion is characterized by a local balance of forces including f, a, g, h, and hence the macroscopic length like the container size is irrelevant [19–21]. In vertically oscillated thin granular layers, regular polygonal cells and

stripes are easily reproduced [1,9–12,23], in which the boundary shape is apparently independent (or at least not important) to the pattern selection. This could be seen clearly when we observe these patterns in a circular container of large extension, which has no preferred direction of the alignment of the cells [23]. The orientation of the sides of these cells met angled to the boundary wall, and it is less than about one-half wavelength that the regularity of the cell pattern is disturbed, which means that the granular layer is in a highly dissipative regime. Then a question arises how these collective motions are generated over the macroscopic size of the cell. Our experiments suggest that the above-mentioned mechanism of pattern formation, inherent to the granular material on a vibrating rigid plane, coherently induces configuration change of particles and dilatation of the layer over the entire bottom plane, which develops into regular patterns irrespective of the boundary shape.

ACKNOWLEDGMENT

This work was partially supported by Grant-in-Aid for Scientific Research (C).

[1] M. Faraday, Philos. Trans. R. Soc. London **52**, 299 (1831).
[2] H. M. Jaeger and S. R. Nagel, Science **255**, 1523 (1992).
[3] H. M. Jaeger, S. R. Nagel, and R. P. Behringer, Rev. Mod. Phys. **68**, 1259 (1996).
[4] J. Duran, *Sables, Poudres et Grains* (Sands, Powder and Grains) (Edition Eyrolles, Paris, 1997) (in French).
[5] S. Douady, S. Fauve, and C. Laroche, Europhys. Lett. **8**, 621 (1989).
[6] C. R. Wassgren, C. E. Brennen, and M. L. Hunt, J. Appl. Mech. **63**, 712 (1996).
[7] Y. Lan and A. D. Rosato, Phys. Fluids **9**, 3615 (1997).
[8] A. Goldshtein, M. Shapiro, L. Moldavsky, and M. Fichman, J. Fluid Mech. **287**, 349 (1995).
[9] F. Melo, P. Umbanhowar, and H. L. Swinney, Phys. Rev. Lett. **72**, 172 (1994).
[10] F. Melo, P. B. Umbanhowar, and H. L. Swinney, Phys. Rev. Lett. **75**, 3838 (1995).
[11] P. Umbanhower, F. Melo, and H. L. Swinney, Nature (London) **382**, 793 (1996).
[12] T. H. Metcalf, J. B. Knight, and H. Jaeger, Physica A **236**, 202 (1997).
[13] E. Clément, L. Vanel, J. Rajchenbach, and J. Duran, Phys. Rev. E **53**, 2972 (1996).
[14] S. Luding, E. Clément, J. Rajchenbach, and J. Duran, Europhys. Lett. **36**, 247 (1996).
[15] E. Clément and L. Labous, Phys. Rev. E **62**, 8314 (2000).
[16] K. M. Aoki and T. Akiyama, Phys. Rev. Lett. **77**, 4166 (1996).
[17] C. Bizon, M. D. Shattuck, J. B. Swift, W. D. McCormick, and H. L. Swinney, Phys. Rev. Lett. **80**, 57 (1998).
[18] Sung Joon Moon, M. D. Shattuck, C. Bizon, Daniel I. Goldman, J. B. Swift, and H. L. Swinney, Phys. Rev. E **65**, 011301 (2002).
[19] A. Ugawa and O. Sano, J. Phys. Soc. Jpn. **71**, 2815 (2002).
[20] A. Ugawa and O. Sano, J. Phys. Soc. Jpn. **72**, 1390 (2003).
[21] K. Kanai, A. Ugawa, and O. Sano, J. Phys. Soc. Jpn. **74**, 1457 (2005).
[22] B. J. Alder and T. E. Wainwright, J. Chem. Phys. **31**, 459 (1959).
[23] O. Sano, A. Ugawa, and K. Suzuki, Forma **14**, 321 (1999).
[24] R. P. Feynman, R. B. Leighton, and M. Sands, in *The Feynman Lectures on Physics* (Addison-Wesley, Reading, MA, 1964), Vol. II, Chap. 38–5.
[25] F. Bowman, in *Introduction to Elliptic Functions with Applications* (Dover, New York, 1961), Chap. II; H. T. Davis, in *Introduction to Nonlinear Differential and Integral Equations* (Dover, New York, 1962), Chap. 6; E. T. Whittaker and G. N. Watson, in *A Course of Modern Analysis*, 4th ed. (Cambridge Univ. Press, Cambridge, England, 1927), Chap. XXII; M. Abramowitz and I. A. Stegun, in *Handbook of Mathematical Functions* (Dover, New York, 1965), Chaps. 16 and 17.